Process Based Large Scale Molecular Dynamic Simulation of a Fuel Cell Catalyst Layer

Xiao, Yu; Yuan, Jinliang; Sundén, Bengt

Published in:
Journal of the Electrochemical Society

DOI:
10.1149/2.028203jes

2012

Process Based Large Scale Molecular Dynamic Simulation of a Fuel Cell Catalyst Layer

Yu Xiao, Jinliang Yuan,[z] and Bengt Sundén

Department of Energy Sciences, Faculty of Engineering,

Lund University, 22100 Lund, Sweden

[z]E-mail: sornxiao@gmail.com

Abstract

In this paper, a large scale molecular dynamic method for reconstruction of the catalyst layers (CLs) in proton exchange membrane fuel cells is developed as a systematic technique to provide an insight into the self-organized phenomena and the microscopic structure. The proposed Coarse-Grained (CG) method is developed and applied to the step formation process, which follows the preparation of the catalyst-coated membranes (CCMs). The fabrication process is mimicked and evaluated in details with consideration of the interactions of material components at a large scale. By choosing three sizes of the unit box, the relevant configurations of the equilibrium states are compared and analyzed. Furthermore, the primary pores of 2-10 nm in the agglomerates mainly consist of the channel space, which acts as the large networks and could be filled with liquid water. Moreover, various physical parameters are predicted and evaluated for four cases. The active Pt surface areas are also calculated by the current model, and then compared with the experimental data available in the literature. Finally, the pair correlation functions are employed to

predict the distributions and hydrophobic properties of the components, providing the information on phase segregation and microscopic structure of the CLs.

Manuscript submitted August 15, 2011; revised manuscript received November 28, 2011. Published xx xx, xxxx.

1 Introduction

The polymer electrolyte membrane fuel cells (PEMFCs) fueled by hydrogen are supposed to be the most suitable successor for the internal combustion engine (ICE) in light duty vehicles, owing to their fast and easy start-up and high efficiency. As one of the key components in PEMFCs, the catalyst layers (CLs) play an important role in the performance and stability of the membrane electrode assemblies (MEAs), which highly depend on the microscopic structure-related properties.[1]

The CLs are porous composites of complex microstructures of the building blocks, i.e., Pt nano-particles, carbonaceous substrates and Nafion ionomers with primary pores of 2-10 nm. Here, the Pt clusters range 2-5 nm and the most commonly employed carbon support, Vulcan XC-72, has a diameter of 20-30 nm. The secondary pores between the agglomerates are in the order of 10-50 nm. All these aggregates are connected by the ionomers to serve as the pathway for the protons generated/consumed in the electrochemical reactions. The typical thickness of a CL ranges from 10 to 30 microns and is a function of the material composition and the fabrication processing.

Due to the limitations of experiments at the extreme small scales, computational modeling is widely used to investigate the transport and electrochemical phenomena

in the CLs. Among these models, there are two different assumptions for the CLs according to the research focus: (i) an infinitely thin-film interface or uniformly distributed agglomerates, which has been used in the macro-homogenous models for the fundamental study of fuel cells; (ii) a homogenous or random heterogeneous nano-porous medium, in which the complex morphologies can be related to relevant effective properties that characterize the transport and reactions at the nano-pores level. For the macroscopic approach,[2, 3] the exact geometric details of the CLs are neglected; thus, only physical properties, such as the porosity, the exchange current density, the matching of the components and thickness of CLs, are considered for the effects on the fuel cell performance. In fact, the CLs are composed of inter-penetrating phases, in which localized percolating features are important. Therefore, the macro-homogenous models without structural resolution could lead to wrong or misleading conclusions for the main detrimental effects on the PEMFC performance. As it is, the (ii) approach becomes more and more important and extensive efforts have been made to reconstruct the microscopic structure of the CLs.

In the latter case, the reconstruction methods need to be developed to evaluate and analyze the critical microstructural features, such as volume fractions and surface areas of specific phases, three-phase boundary (TPB) length, and the connectivity and tortuosity of specific subphases. Thus, the advanced analytical tools are necessary to directly correlate transport and reaction processes with structural details at the microscopic scale and even down to the atomistic level.[4] However the classical scanning methods, such as scanning electron microscopy, can only provide

two-dimensional images of the microstructures;[5] and thus, only limited information can be available on how regions are interconnected in real three-dimensional space. Recently, the application of dual-beam focused ion beam (FIB) scanning electron microscopy has been demonstrated to make a complete three-dimensional reconstruction of a solid oxide fuel cell electrode.[6, 7] Moreover, a kind of fabricating process based reconstruction and simulation method has been performed for the CLs.[8] Through a controlled quasi-random algorithm, the experimental fabrication process is mimicked to provide an insight into the nano-scale properties of transport and the mechanism of electrochemical reactions, e.g., Knudsen diffusion of oxygen in nano-pores, and charge transport in thin-film electrolyte. The Lattice Boltzmann Method (LBM) also provides an effective tool to investigate the transport phenomena at pore-scale level.[9] In CLs, various methods have been developed to describe the diffusion process in complex pore structures,[10, 11] and to study the structure-wettability influence on the underlying two-phase dynamics.[12] The utility of the stochastic reconstruction technique coupled with the direct numerical simulation (DNS) model is also demonstrated through addressing the influence of microstructural inhomogeneity on the fuel cell performance.[13, 14] Some efforts have also been made to simulate species transport and electrochemical reactions in the CLs at the nanometer length scale in a computationally efficient manner.[15] However, there is still a lack of systematic reconstruction techniques to reflect fabricating CLs with controlled microstructures.

Atomic-scale models can predict physical properties of materials with ideal, theoretical or proposed microstructures under clearly defined conditions within the size of several nanometers. However, they are not able to probe the random morphology of the complete CLs due to computational limitations. Therefore, it is expected to use the multiscale simulation strategies to bridge the models and simulation techniques across the atomic-scale to microscale. Several approaches have been proposed, such as Dissipative Particle Dynamics (DPD) method[16, 17] and Coarse-Grained (CG) molecular simulation.[18, 19] In the CG method, super-atoms are used to represent groups of atoms, and interactions are only defined between these super-atoms. Thus, a reduction of the number of degrees of freedom is achieved. At the same time it can consolidate the major features of microstructure formation in the CLs of PEMFCs. In this way, the complete description of the CLs microscopic structure can broaden the range of length scales from the chemical bond (at around one angstrom in length) up to chain aggregates, extending for many hundreds of angstroms and beyond, so-called large scale molecular dynamics (MD) method.

In this work, a large scale MD simulation method (based on the CG model) is developed as a systematic technique to provide an insight into the self-organized phenomena and the microscopic structure of the CLs, based on the experimental fabrication procedure.[20] The main purpose of this work is to improve the understanding of the step formation process and the fabrication technique that allows control of the structures, with consideration of the interactions of the Pt/carbon aggregates, Nafion ionomers and water at a large scale. After a description of the

methodology, the final microstructures are presented and analyzed by the MD package, which is primarily designed for biomolecular systems such as proteins and lipids. Moreover, the volumes of the pores and the active Pt surface areas are further evaluated and compared with the experimental data, together with the distribution and hydrophilic features of the components.

2 Methodology

2.1 CG beads and their properties

In this study, the CG method is employed to reconstruct the microscopic structure of the CLs in two major steps: ① Introduce and construct the Nafion chains, water and hydronium molecules, carbon and Pt particles with corresponding spherical beads at a predefined length scale; ② Specify the parameters of renormalized interaction energies between the distinct beads as the MARTINI force field,[21, 22] which has been widely used and proved in the applications of lipid,[23] polymers [24] and carbohydrates.[25] For the defined beads in step ①, four types of interaction sites are mainly considered in step ②: polar (P), nonpolar (N), apolar (C) and charged (Q). The polar sites represent neutral groups of atoms, the apolar sites are hydrophobic moieties, and the nonpolar groups are used for mixed groups, which are partly polar and partly apolar. The charged sites are reserved for ionized groups. For particles of type N and Q, subtypes are further distinguished by a letter denoting the hydrogen-bonding capabilities (d=donor, a=acceptor, 0=not exist). The defined types of all components are presented in table 1.

In this CG model, the nonbonded interactions between sites i and j are described

by the Lennard-Jones (LJ) potential, which has become a standard procedure in the MD simulations

$$V_{LJ}(r) = 4\varepsilon_{ij}\left[\left(\frac{\sigma_{ij}}{r}\right)^{12} - \left(\frac{\sigma_{ij}}{r}\right)^{6}\right] \quad [1]$$

In Eq. 1, ε_{ij} represents the depth of the potential at the minimum ($r_{min} = 2^{1/6}\,\sigma_{ij}$) and σ_{ij} is the point at which $V_{LJ} = 0$. In analogy to the case in Ref.[26], only five levels of interactions (determined by the pair of bead types) are considered in this study: attractive (I, ε_{ij}=5 kJ mol^{-1}), semiattractive (II, ε_{ij}=4.2 kJ mol^{-1}), intermediate (III, ε_{ij}=3.4 kJ mol^{-1}), semirepulsive (IV, ε_{ij}=2.6 kJ mol^{-1}) and repulsive (V, ε_{ij}=1.8 kJ mol^{-1}). For all five interaction types the same effective bead diameter is assumed, σ_{ij} = 0.43 nm. The LJ parameters, $4\varepsilon_{ij}\sigma_{ij}^{6}$ and $4\varepsilon_{ij}\sigma_{ij}^{12}$, can be calculated based on the level of interactions. For example, carbon slabs are partially hydrophobic, semi-repulsive interaction with water and Nafion side chains, but semi-attractive interaction with other carbon and Pt beads as well as with Nafion backbones.[27] All the interactions between each two type of beads have been defined and proved in Ref [21, 22], and in this work, a cutoff of 1.2 nm is also used for the LJ interaction potential.[10, 26] To reduce the cutoff noise, the LJ potential is smoothly shifted to zero between a distance r_{shift} = 0.9 nm and r_{cut}. With the standard GROMACS shift function (Φ), both the energy and the force vanish at the cutoff distance.[26, 28]

$$\Phi_\alpha(r) = \frac{1}{r^\alpha} - \frac{A}{3}\left(r - r_{shift}\right)^3 - \frac{B}{4}\left(r - r_{shift}\right)^4 - C; \quad r_{shift} \le r \le r_{cut} \quad [2]$$

$$\Phi_\alpha(r) = \frac{1}{r^\alpha} - C; \quad r \le r_{shift} \quad [3]$$

$$A = \frac{\alpha\{(\alpha+1)r_{shift} - (\alpha+4)r_{cut}\}}{r_{cut}^{(\alpha+2)}\left(r_{cut} - r_{shift}\right)^2} \quad [4]$$

$$B = -\frac{\alpha\{(\alpha+1)r_{shift} - (\alpha+3)r_{cut}\}}{r_{cut}^{(\alpha+2)}(r_{cut} - r_{shift})^3} \quad [5]$$

$$C = \frac{1}{r_{cut}^{\alpha}} - \frac{A}{3}(r_{cut} - r_{shift})^3 - \frac{B}{4}(r_{cut} - r_{shift})^4 \quad [6]$$

here α denotes the power of the respective LJ (α=6,12) or Coulombic (α=1) terms.

In addition to the LJ interactions, the interactions between charged groups (type Q) are evaluated via the normal electrostatic Coulomb potential:

$$V_{el}(r) = \frac{q_i q_j}{4\pi\varepsilon_0\varepsilon_r r} \quad [7]$$

with relative dielectric constant ε_r=20 for explicit screening. Shifting of the electrostatic potential in this manner reflects the effect of a distance-dependent screening.

Bonded interactions between the chemically connected sites are described by a week harmonic potential $V_{bond}(R)$ with the equilibrium distance (the same as σ_{ij}, 0.43 nm)

$$V_{bond}(R) = \frac{1}{2}K_{bond}(R - R_{bond})^2 \quad [8]$$

The LJ interaction is excluded between the bonded particles, but included between the second nearest neighbors. The force constant of the harmonic bonding potential is K_{bond}=1250 kJ mol^{-1} nm^{-2}. To represent chain stiffness, a weak harmonic potential $V_{angle}(\theta)$ of the cosine type is introduced for the angles:

$$V_{angle}(\theta) = \frac{1}{2}K_{angle}\{\cos(\theta) - \cos(\theta_0)\}^2 \quad [9]$$

where the basic equilibrium bond angle θ_0 is 180°, with a force constant of K_{angle}=25 kJ mol^{-1} rad^{-2}. Such a small force constant allows an angle deviation of 30°, which reproduces the properties of Nafion chains [21].

2.2 Mapping in the CG model

The MD method above is implemented by the GROMACS package,[29] which is primarily designed for biochemical molecules like proteins, lipids and nucleic acids that have a lot of complicated bonded interactions. However, because GROMACS is extremely fast at calculating the nonbonded interactions, many research groups are also using it for research on non-biological systems, such as the polymers.[28, 30] In this work, the whole CG model of Nafion copolymer, as shown in Fig. 1, includes a part of the atomistic level configuration of a Nafion chain. According to Ref.[4], a side chain unit in the Nafion ionomer has a molecular volume of 0.306 nm^3, which is comparable to the molecular volume of a four-monomer unit of poly(tetrafluoro-ethylene) (PTFE) (0.325 nm^3). Therefore, one side chain and four-monomer unit (-$(CF_2CF_2)_4$-) are coarse-grained as spherical beads of volume 0.315 nm^3 (r=0.43 nm). The Nafion oligomer consists of 20 repeated monomers;[20] therefore, there are 20 side chains, with the total length of ~30 nm. The repeated monomers are represented by two blue apolar beads (C) as the hydrophobic backbone and one yellow charged bead (Qa) as the hydrophilic side chain, as shown in the shaded rings in Fig. 1.

Carbonaceous particles can be coarse-grained in various ways;[4] in this work, the CG potential parameters are systematically obtained from the atomistic-level interactions. In Fig. 2a, the carbon slab is firstly constructed by the Atomistic Simulation Environment (ASE) software,[31] which provides python modules for manipulating atoms, analyzing simulations, visualization etc. ; because it is more easy and accurate to create the structure without getting lost in the volume of

information.[32] The density functional theory (DFT) calculations of the carbon slab are performed by the Jacapo calculator, which is an ASE interface for Dacapo and fully compatible with ASE. In the Jacapo, the ultrasoft pseudopotentials are used to describe the interactions between valence and core electron, and the wave functions are expanded in plane waves with the kinetic energy cutoff of 350 eV.[33, 34] To describe the electron exchange-correlation interaction, generalized gradient approximation with Perdew-Wang (PW91) function is adopted.[35] The carbon slab is modeled by eight layers of the zigzag graphene structure, and each layer has a regular hexagonal net of carbon atoms with the C-C bond length of 1.42 Å. The interlayer spacing is equal to 3.35 Å and the layers are interacted by van der Waals force.[30] In the following step, the CG Builder from VMD (Visual Molecular Dynamics) software[36] is employed to provide a shape-based coarse graining (SBCG) tool for transforming structures from all-atom representations to CG beads.[37, 38] Based on a neural network learning algorithm,[39] the shape-based method is used to determine the placement of the CG beads, which also have masses correlated to the clusters of the represented atoms. Neighboring beads are connected by harmonic springs, while separate molecules interact through non-bonded forces (Lennard-Jones and Coulomb potentials).[37] Interactions are parameterized on the basis of all-atom simulations and available experimental data. Therefore, there are 36 carbon atoms in one bead of the slab (r=0.43 nm), as shown by the shaded rings in Fig. 2b. By this method, the typical carbon slab with the size of 5×5×2.5 nm^3 is represented by 224 nonpolar beads (type of N).

The Pt nano-clusters supported on carbon slabs are also considered in this work. For the Pt/C sample prepared in Ref.[40], the majority of the Pt particles are in the range of 2-3 nm (an average size of 2.4 nm). According to Ref.[41], it is envisaged that the fcc-like clusters will occur at this size. Similar to the carbon slabs, the Pt nano-cluster is firstly constructed by the ASE software and then coarse-grained by the VMD software. Thus, the 10×10×6 fcc-Pt (111) cluster is represented by 30 nonpolar beads (type of Na) in Fig. 3a. Therefore, each bead consists of 20 Pt atoms with the radius of 0.43 nm, as shown by the shaded rings in Fig. 3a. In Fig. 3b, four water molecules are represented as one single polar CG site (type of P) with the radius of 0.43 nm. For the electroneutrality condition, three water molecules plus a hydronium ion are also added into the system and represented by one charged bead (type of Qd) of radius 0.43 nm.

2.3 Target box and assumptions

Three different sizes of the simulation boxes are studied as shown in table 2, and these boxes can be assumed as the typical units of the CLs. Taking the case 1 as an example: the initial simulation box has a size of 25×25×25 nm^3, with the periodical boundary conditions (PBC) at all the faces of the volume unit. It includes 15 carbon slabs (3360 carbon beads), 8 Pt clusters (240 Pt beads), and 50 Nafion oligomers. A total of 1000 CG hydronium ions are added for electroneutrality. The number of water beads is fixed at a value corresponding to approximately 13 water molecules per side chain (i.e., λ=13,[4] corresponding to 3250 water beads). For this case, there are nearly 10000 CG particles totally. However, the addition of all these components is followed by the experimental fabrication process of the CLs, as explained in the following

section.

2.4 Experimental procedures for preparation of the CLs

The Pt/C electrocatalysts (40 wt%, BASF) are firstly weighed, and then wetted with the distilled water. After ultrasonic treatment for 30 min, Nafion® perfluorinated resin solution (5 wt% in lower aliphatic alcohols and water, containing 15-20 wt% water) is added to the catalyst ink and stirring is kept to reach a well-distributed condition. After heating and drying to remove excess water and other impurities, the Nafion concentration is kept 32~38 wt%, in the range of a typical value used in the CLs.[4, 11] For the cases of 2 and 3, the proportion of the components is the same as that in the case 1.

2.5 Simulation parameters

For every fabrication process, the centers of the beads are randomly placed on cubic lattice points in the initial stage. Firstly, the initial structure is optimized for 250 ps at T_0=320 K, using 25 fs time steps in the course of a step integration procedure. This short energy minimization displaces the overlapped beads at beginning. Then, the equilibrium of this resulting configuration is achieved by the annealing procedure.[42] The temperature is controlled by the Berendsen algorithm,[43] which simulates a weak coupling to an external heat bath with the given temperature. The weak coupling algorithm is applied separately for each component (Nafion, carbon slabs, Pt clusters and water beads) with a time constant of 1.0 ps and a reference temperature T_0. The system is further expanded over a period of 3.0 ps by gradually increasing the temperature from 300 to 325 K. After that, the MD simulation is

employed for another 3.0 ps in a canonical (NTV) ensemble,[4] followed by a cooling procedure to 300 K. During the simulation, the information and data are saved every 1000 steps (40 ps) and used for later analysis. All these simulations are performed with the GROMACS simulation package version 4.5.3.[29]

3 Results and Discussion

3.1 Process based reconstruction

In this study, numerical reconstruction of a CL is performed through the CG method by the GROMACS package, mimicking the experimental fabrication process.[44] Take the case 1 in table 2 as an example: In step i, the Pt/C catalyst (40 wt%, BASF) nanoparticles, represented by 15 carbon slabs and 8 Pt clusters, are randomly dispersed in the 25×25×25 nm^3 box, which is filled up with water beads in the following. The CG method is then performed by GROMACS as described in section 2.4. After MD running for 10 ns to mimic the ultrasonic treatment in the experimental process, the final formation configuration is obtained for the equilibrium state, as shown in Fig. 4_ia. For better clarity, only the carbon slabs and the Pt clusters are shown and the phenomenon of self-aggregation is easily observed. In view of the PBC, the two main agglomerates come together actually. Furthermore, it is found that the Pt clusters are deposited on the carbon agglomerates and their lateral parts adsorb on the carbon surface (see Fig. 4_ib). In step ii, 50 Nafion chains and excess water beads, including 1000 hydronium ions (to keep the electroneutrality condition), are added to the box. After MD running for 10 ns to mimic the mixing process, it is clearly found that the ionomer backbones assemble into a separate interconnected

phase in the void spaces of the Pt/C aggregates, as shown in Fig. 4_iia (the solvents are invisible for better clarity). For a better view of the generated structures, the target box is duplicated by 2×2, as shown in Fig. 4_iib. Therefore, it is easy to get the network connections of Nafion chains. In the final step iii, excess water beads are removed due to the heating and drying process for CLs (the heating process is not taken into account in the simulation, but the self-assembling processes for the CLs in the final state are considered and the reference temperature is set to 300 K). Therefore, all the components of a CL can be expressed in the final equilibrium state (see Fig. 4_iiia, after MD running for 50 ns), and the number of water beads is 2250 (including 1000 beads with the hydronium ions), corresponding to 13 waters per side chain. In Fig. 4_iiib, the 3×3×1 schematic drawing of the target box (75×75×25 nm^3 in total) is shown for better understanding the secondary pores of about 40 nm in length among the agglomerates.

Following the same way to reconstruct the stable configurations for the cases above, and the final equilibrium state of the case 2 is obtained for a box of 50×25×25 nm^3, as shown in Fig. 5 (t=50 ns). As expected, all these particles coalesce to form the agglomerate, which is constructed by the carbon slabs and the Pt clusters, surrounded by ionomers and water beads. In Fig. 5a, the agglomerated carbon slabs deposited with Pt clusters are clearly observed. These linked carbons provide the routes for the electrons to the adsorbed Pt clusters. Furthermore, the ionomer backbones assemble into a separate interconnected phase in the void spaces, while the side chains tend to be located at the interfaces between the ionomer domains and the water-filled pores.

The ionomer molecules do not penetrate into the Pt/C clusters; instead, they form proton-conducting volume elements that are connected to the surface of the aggregates.[4] Some primary pores are clearly displayed in the range of 2-10 nm, together with the secondary pores between the agglomerates with the sizes of 10-50 nm. From the image, it is also evident that the Nafion ionomers cover the surface of the Pt/C aggregate instead of penetrating into the individual particles. In Fig. 5b, the total energy changes for the three cases are presented against the MD running time. It is easy to understand that a larger box takes longer time to reach the stable state.

3.2 Microscopic parameters evaluation

As mentioned above, there are lots of the voids and the pore spaces in the agglomerate, which are more intricate and complicated for a big size box (50 nm×50 nm×50 nm), as shown by the final image (t=50 ns) in Fig. 6a. The Voss Volume Voxelator (3V) web server provides a technique that can obtain the overall shape of the channels.[45] It uses the rolling probe method,[46] which essentially works by rolling a virtual probe or ball of a given radius around the surface of a macromolecule or the agglomerate to calculate the volumes. When a probe of zero size is used, the van der Waals radius is obtained. For the CG system, the effective bead diameter (σ_{ij}) is 0.43 nm; therefore, the particle volume (V) can be calculated by rolling the probe with the radius of 4.3 Å. For the case 3, the particle volume (V) is 14650 nm^3, and its surface is marked in pink as shown in Fig. 6b. However, as the probe radius increases, the surface features are filled in. In order to distinguish the interior of the agglomerate from its exterior, the agglomerate volume (V_0) is defined here as the space inside the

limiting surface of the agglomerate with a larger probe radius. For the probe radius of 4 nm, which is appropriate for the primary pore analysis, the convex hull is obtained and marked in blue (see Fig. 6c).

The difference between the agglomerate volume (V_0, blue) and the particle volume (V, pink) constitutes the primary pore spaces of the CLs, and a part of it is shown in Fig. 6d. Close to the solid surface of the agglomerate, there are mainly two types of internal spaces: cavities and channels. The cavity is the space large enough to accommodate a water molecule, but isolated by the Pt/C aggregates, as shown in Fig. 6d. It is not connected to the agglomerate exterior but regarded as the dead zone for the electrochemical reactions. The second type of internal space is loosely defined as the "channel space" (see Fig. 6d), which includes surface invaginations, grooves, pockets, or clefts, as well as long internal channels, large chambers and deep pores. In practice, it is difficult to segregate a channel from a cleft or a pocket without detailed analysis of the surface. For the CLs, the channel space, which is a major part of the primary pores, acts as a large network within the agglomerates and can be easily filled with liquid water by the capillary force. It is also the place where the ionomer clusters are able to penetrate into, and thus has more influences on the proton conduction. The channel volume (V_{chanel}) can be distinguished and calculated by the tools in the 3V web server, [45] and the results are presented in table 3. In addition, the real density ρ , which can be expressed as the mass (M) of a unit box divided by the particle volume (V), should be almost the same for the cases 1-3, as shown in table 3.

3.3 Model Validation

In order to obtain optimized catalytic activity and reduce overall system cost, Pt is generally dispersed as nano-sized particulates to get higher electrochemical active surface areas (EAS).[47] The active Pt surface areas of a commercial 20 wt% Pt/C catalyst (E-TEK) are measured by both hydrogen adsorption and CO-stripping voltammetry.[48, 49] To compare with these experimental data, the configuration of the corresponding CLs is reconstructed in the 50×50×50 nm^3 unit volume, as the case 4 in table 2. In the box, there are 120 carbon slabs, 25 Pt clusters, 400 Nafion oligomers and 26000 water beads in the simulation box with PBC at all the faces. Based on the step formation process, the final equilibrium state is obtained after MD running for 50 ns. In GROMACS, the information of each component can be separated and exported individually. Thus, by rolling the probe with the radius of 0.43 nm,[46] the surface of the Pt clusters is obtained, as shown in Fig. 7a; at the same time, the total surface area (A_1) and volume (V_1) of the Pt clusters are calculated, as shown in table 4. Most of these Pt nano-particles are well-dispersed among the agglomerates, and only two clusters hold together obviously. With the same method, the surface of the carbon slabs is plotted in Fig. 7b; while the overall figure of the Pt/C aggregate is enlarged in Fig. 7c. The related geometry parameters (A_2, V_2 and A_{12}, V_{12}) can be obtained, as outlined in table 4. In Fig. 7c, some parts of the Pt clusters embed into the carbon aggregate and lose their electrochemical activities. Therefore, the embedded parts of the surfaces have no contribution to the EAS and should be excluded.

In order to calculate the active Pt surface area (A_s), the Pt and C boundary is abstracted as a whole Pt particle (A_1, V_1), embedding into one big carbon slab (A_2,

V_2), as shown in Fig. 7d. When the total surface areas and volumes are provided from the table 4, two relations can be deduced from the geometry,

$$A_s+A_2=A_{12}+A_{if} \quad [10]$$

$$V_1 + V_2 - V_{12} = \iint_{A_{if}} H_e dA \quad [11]$$

where A_{if} is the boundary interface area and H_e represents the effective height of embedding part. Due to the lack of the function expressions for the real Pt particles, Pt is ideally assumed as a cylinder, which is perpendicular to the carbon slab interface for simplicity. Then, another constrain can be obtained as follows,

$$\frac{H - H_e}{H} = \frac{A_s - \frac{V_1}{H}}{A_1 - \frac{V_1}{H} - A_{if}} \quad [12]$$

where H represents the cylinder height and can be calculated from A_1 and V_1.

$$A_1 = 2\pi R^2 + 2\pi R \cdot H \quad [13]$$

$$V_1 = \pi R^2 \cdot H \quad [14]$$

The predicted results, including the case 3 for comparison, are listed in table 5. From the assumed perpendicular cylinder model, each case has two real solutions, which have distinct shapes (H and R are quite different), but similar active surface (A_s) and interface areas (A_{if}). Thus there will be the approximate results of the active Pt surface areas per gram catalyst, which are little affected by the Pt shapes and the model assumptions.

In table 6, the three-dimensional volume of the Pt unit is about 2.8×2.3×sin60° nm^2 (crystal plane) ×1.4 nm (height) in the simulation work. However, some of these Pt units are very close to each other (see Fig. 7a), and can be assumed as the whole

particles, when observed in the experiments. In fact, the average sizes of the Pt particles in the modeling are bigger than the Pt unit and quite close to the values from the experiments. In this case, the average active Pt surface areas of the cases 3 and 4, which own different Pt mass percentage but similar Pt average sizes, agree reasonably with the experimental ones.[47-49]

3.4 Hydrophobic properties

Pair correlation function (PCF, or Radial Distribution Function RDF), $g(r)_{ij}$, is usually used to evaluate the probability of finding the center of a particle at a given distance, r, from the center of another particle. For short distances, PCF is related to how the particles are packed together. In this work, the structural correlation function between distinct components of the CLs is used to provide the information on phase segregation and microscopic spatial structure in the CLs. In Fig. 8, the PCFs of the case 3 are shown for the equilibrium configuration of the CLs in the vacuum environment, including Pt clusters (Pt), side chains (S) and backbones (B) of Nafion ionomer, carbon slabs (C) and water beads (W). These functions are applied in terms of the deposition of Pt clusters on the carbon slabs, the segregation of Nafion ionomers and Pt/C aggregates into distinct domains, distributions of water and hydronium ions (with respect to side chains and backbones of Nafion), and also the TPB regions.

The PCFs in Fig. 8a exhibit typical characteristics of the uneven density system of the interacting particles in the case 3. At the short distance ($r < 2$ nm), the PCFs are enhanced, which is indicated by sharp primary peaks and distinct secondary peaks.

These features attribute to the Lennard-Jones interactions, working at short distance. The primary peak of W-W autocorrelation function occurs at roughly 0.5 nm (slightly higher than the radius of beads), and has a height of 75. This means that the relative density of water beads is almost 75 times higher if the distance from another water bead is 0.5 nm. It reveals a fact of the highly non-uniform distribution and gathering features of the water beads. A similar structure is exhibited for the side chains, g_{SS}, and the hydronium ions g_{WhWh}. This indicates a strong clustering due to the aggregation and folding of polymer backbones. The separation of the primary peaks of the three components is determined by the interaction forces between the pair beads. For example, g_{WhWh} is smaller than g_{WW} in the primary peak region due to electrostatic repulsion between the charged hydronium ions. Fig. 8b exhibits the hydrophobic/hydrophilic properties of the components in the CLs. The primary peak of the function g_{SW} indicates that the side chains are mostly surrounded by water with the hydrophilic feature, while other species with the functions g_{CW}, g_{BW} and g_{PW} are more hydrophobic than the side chains, due to $g_{CW} > g_{BW} > g_{PW} > g_{SW}$.

4 Conclusions

In this study, a systematic technique based on CG method is developed to provide vivid predictions of self-assembling processes for the CLs in PEMFCs. This technique is based on step formation process and allows control of the structures with considering the interactions of the Pt/carbon aggregates, Nafion ionomers and water at a large scale. In particular, three different sizes of the target boxes are investigated, and then the microstructures at the equilibrium state are presented and analyzed by the

MD packages. As expected, the ionomer backbones are attached to the surface of Pt/C agglomerates; and the side-chains are buried inside hydrophilic domains with a weak contact to carbon domains, where the protons on the sulfonic acid groups can "hop" from one acid site to another.[50]

In the final configuration (after MD running for 50 ns), the primary pore spaces are clearly observed in the range of 2-10 nm, based on the volume difference between the agglomerate space and the particle space. By the rolling-probe method, the physical parameters of the CLs are evaluated and further used to calculate the real densities of the agglomerates, which are similar for different box sizes with the same components. The active Pt surface areas in the two cases are further calculated by the current model, and then compared with the experimental data with a reasonable agreement. In addition, the PCFs are employed to confirm the typical hypothesis, i.e., the carbon slabs form the agglomerates and the hydrated ionomers form a separate phase attaching to the surface of carbon agglomerates.

In principle, the process based CG method can provide various microscopic parameters from the reconstructed microstructures, which are relating to the important properties and parameters in the upper scale models, for comprehensive understanding of the multifunctional porous materials and the effects on various transport processes and the reactions in the fuel cell systems.

Acknowledgment

The European Research Council (ERC, 226238-MMFCS) supports the current

research.

References

1.L. M. Hall, A. Jayaraman and K. S. Schweizer, *Current Opinion in Solid State and Materials Science*, **14**, 38.

2.V. A. Paganin, C. L. F. Oliveira, E. A. Ticianelli, T. E. Springer and E. R. Gonzalez, *Electrochimica Acta*, **43**, 3761 (1998).

3.S. M. Chang and H. S. Chu, *Journal of Power Sources*, **161**, 1161 (2006).

4.Q. H. Zeng, A. B. Yu and G. Q. Lu, *Progress in Polymer Science*, **33**, 191 (2008).

5.R. W. James, K. Worawarit, M. Roberto, C. Hsun-Yi, M. H. Jon, J. M. Dean, T. Katsuyo, W. V. Peter, B. A. Stuart and A. B. Scott, *Nature Materials*, **5**, 541 (2006).

6.C. Ziegler, S. Thiele and R. Zengerle, *Journal of Power Sources*, **196**, 2094 (2011).

7.B. Cotterell, J. Y. H. Chia and K. Hbaieb, *Engineering Fracture Mechanics*, **74**, 1054 (2007).

8.N. A. Siddique and F. Liu, *Electrochimica Acta*, **55**, 5357 (2010).

9.L. Hao and P. Cheng, *Journal of Power Sources*, **195**, 3870 (2010).

10.N. Sheng, M. C. Boyce, D. M. Parks, G. C. Rutledge, J. I. Abes and R. E. Cohen, *Polymer*, **45**, 487 (2004).

11.Y. Dong, D. Bhattacharyya and P. J. Hunter, *Composites Science and Technology*, **68**, 2864 (2008).

12.M. Fermeglia and S. Pricl, *Computers & Chemical Engineering*, **33**, 1701 (2009).

13.P. P. Mukherjee and C. Wang, *Journal of The Electrochemical Society*, **153**, A840

(2006).

14.S. H. Kim and H. Pitsch, *Journal of The Electrochemical Society*, **156**, B673 (2009).

15.K. J. Lange, P. Sui and N. Djilali, *Journal of The Electrochemical Society*, **157**, B1434 (2010).

16.G. Dorenbos and Y. Suga, *Journal of Membrane Science*, **330**, 5 (2009).

17.M. Liu, P. Meakin and H. Huang, *Journal of Computational Physics*, **222**, 110 (2007).

18.S. Izvekov and A. Violi, *Journal of Chemical Theory and Computation*, **2**, 504 (2006).

19.S. Collins, M. Stamatakis and D. Vlachos, *BMC Bioinformatics*, **11**, 218 (2010).

20.J. Cho, J. J. Luo and I. M. Daniel, *Composites Science and Technology*, **67**, 2399 (2007).

21.S. J. Marrink, A. H. de Vries and A. E. Mark, *The Journal of Physical Chemistry B*, **108**, 750 (2004).

22.S. J. Marrink, H. J. Risselada, S. Yefimov, D. P. Tieleman and A. H. de Vries, *The Journal of Physical Chemistry B*, **111**, 7812 (2007).

23.H. J. Risselada and J. Marrink Siewert, *Proceedings of the National Academy of Sciences of the United States of America*, **105**, 17367 (2008).

24.L. Hwankyu, H. d. V. Alex, M. Siewert-Jan and W. P. Richard, *The Journal of Physical Chemistry B*, **113**, 13186 (2009).

25.C. A. López, A. J. Rzepiela, A. H. d. Vries, L. Dijkhuizen, P. H. Hu□nenberger

and S. J. Marrink, *Journal of Chemical Theory and Computation*, **5**, 3195 (2009).

26.D. Porter, *Materials Science and Engineering A*, **365**, 38 (2004).

27.K. Malek, M. Eikerling, Q. Wang, Z. Liu, S. Otsuka, K. Akizuki and M. Abe, *The Journal of Chemical Physics*, **129**, 204702 (2008).

28.Q. Liu and D. De Kee, *Journal of Non-Newtonian Fluid Mechanics*, **131**, 32 (2005).

29.*http://www.gromacs.org/*.

30.G. Scocchi, P. Posocco, A. Danani, S. Pricl and M. Fermeglia, *Fluid Phase Equilibria*, **261**, 366 (2007).

31.*https://wiki.fysik.dtu.dk/ase/overview.html*.

32.B. Wang, X. Ma, C. Marco, S. Renald and W. X. Li, *Nano Letters*, **11**, 424 (2011).

33.B. Hammer, L. B. Hansen, oslash and J. K. rskov, *Physical Review B*, **59**, 7413 (1999).

34.D. Vanderbilt, *Physical Review B*, **41**, 7892 (1990).

35.P. E. Blöchl, *Physical Review B*, **50**, 17953 (1994).

36.*http://www.ks.uiuc.edu/Research/vmd/*.

37.A. Arkhipov, P. L. Freddolino and K. Schulten, *Structure (London)*, **14**, 1767 (2006).

38.A. Arkhipov, P. L. Freddolino, K. Imada, K. Namba and K. Schulten, *Biophysical Journal*, **91**, 4589 (2006).

39.X. Wang, Z. Jin, G. Shen and D. Tang, *Proceedings of the 4th World Congress on Intelligent Control and Automation*, **3**, 2030 (2002).

40.S. Boutaleb, F. Zairi, A. Mesbah, M. Nait-Abdelaziz, J. M. Gloaguen, T. Boukharouba and J. M. Lefebvre, *Procedia Engineering*, **1**, 217 (2009).

41.S. Sinha Ray and M. Okamoto, *Progress in Polymer Science*, **28**, 1539 (2003).

42.X. Yong and G. A. Mansoori, *International Journal of Molecular Sciences*, **11**, 288 (2010).

43.M. Khalili, A. Liwo, A. Jagielska and H. A. Scheraga, *The Journal of Physical Chemistry. B*, **109**, 13798 (2005).

44.V. A. Buryachenko, A. Roy, K. Lafdi, K. L. Anderson and S. Chellapilla, *Composites Science and Technology*, **65**, 2435 (2005).

45.M. Fermeglia and S. Pricl, *Progress in Organic Coatings*, **58**, 187 (2007).

46.L. Sun, R. F. Gibson, F. Gordaninejad and J. Suhr, *Composites Science and Technology*, **69**, 2392 (2009).

47.M. Cai, M. S. Ruthkosky, B. Merzougui, S. Swathirajan, M. P. Balogh and S. H. Oh, *Journal of Power Sources*, **160**, 977 (2006).

48.D. H. Lim, W. D. Lee and H. I. Lee, *Catalysis Surveys from Asia*, **12**, 310 (2008).

49.E. N. Coker, W. A. Steen, J. T. Miller, A. J. Kropf and J. E. Miller, *Microporous and Mesoporous Materials*, **101**, 440 (2007).

50.K. A. Mauritz and R. B. Moore, *Chemical Reviews*, **104**, 4535 (2004).

Table 1 Defined CG beads

CG beads	Color	Represented atoms	Symbol	Specified Type	Radius /nm
1	Yellow	-O-$CF_2CF(CF_3)$-... -O-CF_2CF_2-SO_3H	SO	Qa	0.43
2	Blue	-$(CF_2CF_2)_3$-CF_2-	C1	C	0.43
3	Blue	-$(CF_2CF_2)_4$-	C1	C	0.43
4	Green	4×H_2O	W	P	0.43
5	Magenta	3×H_2O+H_3O^+	Wh	Qd	0.43
6	Gray	36×C	C	N0	0.43
7	Golden	20×Pt	Pt	Na	0.43

Table 2 Cases studied based on different sizes of the target boxes.

Cases	**3-D sizes** /(nm×nm×nm)	**Number of component units in different cases**			
		Carbon slabs	Pt clusters *	Nafion chains	Water beads (including H_3O^+)
1	25×25×25	15	8	50	3250 (1000)
2	50×25×25	30	16	100	6500 (2000)
3	50×50×50	120	65	400	26000 (8000)
4	50×50×50	120	25	400	26000 (8000)

* The mass percentage of Pt is kept to about 40 wt% for the cases 1~3 and 20 wt% for the case 4 in the Pt/C catalyst.

Table 3 Calculated physical parameters of the CLs

Cases	**M** / 10^{-18} g	**V** / nm^3	**V_0** / nm^3	**$V_{Channel}$** / nm^3	**ρ** /(g cm^{-3})
1	6.23	1894	2574	644	3.29
2	12.46	3717	7063	3061	3.35
3	49.80	14650	26795	10004	3.39
4	41.32	13060	20290	6326	3.16

Table 4 Predicted volume and surface area of Pt clusters, carbon slabs and PtC aggregates in an equilibrium state

	j	**V_j (/ nm^3)**	**A_j (/ nm^2)**
Case 3	Pt	595.8	1859
	C	8478	10620
	PtC	9041	12060
Case 4	Pt	281.2	772.7
	C	8035	10120
	PtC	8247	10400

Table 5 Active Pt surface area predicted by the current model

	Solution	R / nm	H / nm	A_s / nm^{-2}	A_{if} / nm^{-2}	Active Pt surface area / ($m^2 g^{-1}$)
Case 3	1	16.9	0.7	1628.1	188.1	51.04
	2	0.6	460.3	1602.8	162.9	50.25
Case 4	1	10.7	0.8	503.0	223.0	20.85
	2	0.7	167.5	452.7	172.7	18.76

Table 6 Comparison of the active Pt surface area

Name	**Pt mass percentage**	**Pt unit or Average size**	**Active Pt surface area** / (m^2 g^{-1})		**Remarks**
			Current study	**Exp***	
Case 3	40 wt%	2.8×2.3×sin60° ×1.4 nm^3	**50.7**	---	Current study
TKK	46.6 wt%	3.6 nm	**---**	**41.9**	Ref [46]
Case 4	20 wt%	2.8×2.3×sin60° ×1.4 nm^3	**19.8**	---	Current study
E-TEK	20 wt%	3.3 nm	**---**	**37.2**	Ref [47, 48]

* Pt/C catalyst (TKK) by CO-stripping voltammetry; Pt/C catalyst (E-TEK) by H_2 desorption cyclic voltammogram

Figure 1. Schematic drawing of the complete Nafion copolymer, which is composed of apolar beads (blue) and charged beads (yellow), and also a part of the atomistic level configuration of a Nafion chain. Four-monomer unit (-$(CF_2CF_2)_4$-) is represented by one blue bead as the hydrophobic backbone, while the side chain (-O-$CF_2CF(CF_3)$-O-CF_2CF_2-SO_3H) with the sulfonic acid group is expressed as one yellow bead with hydrophilic property.

Figure 2. (a) Structural drawing of one carbon slab generated by ASE software, which consists of eight layers of the zigzag graphene structure with a regular hexagonal net of carbon atoms. The interlayer spacing is equal to 3.35 Å. (b) Coarse grain representations of the carbon slab, in which there are 36 carbon atoms in each bead. The typical carbon slab with the size of 5×5×2.5 nm^3 is reconstructed by 224 nonpolar beads (type of N).

Figure 3. (a) Atomistic (in the shaded rings) and coarse grain representation of one

fcc-Pt(111) cluster. The 10×10×6 Pt cluster is represented by 30 nonpolar beads, and each bead contains 20 Pt atoms. (b) A total of four water molecules (or three water molecules plus a hydronium ion) are represented by one CG bead of radius 0.43 nm.

Figure 4. Experimental fabrication process related reconstruction of a CL: Step i: randomly disperse Pt/C catalyst in the 25×25×25 nm^3 box and then the self-aggregation will happen in (a), and the partial enlarged details are shown in (b). Step ii: (a) add the Nafion chains to form the ion transport network and the 2×2 schematic drawing is shown in (b) based on PBC. Step iii: (a) evaporate the residual solvent and exhibit the final image of the equilibrium state at t=50 ns and the 3×3 schematic drawing is shown in (b) based on PBC. In these images, Golden: Pt, Grey: Carbon, Yellow and Blue: Side chain and backbone of Nafion ionomer, Green: Water, Magenta: Hydronium ions, as listed in table 1.

Figure 5. (a) Images of the final equilibrium states after MD running for 50 ns in case 2 with the box size of 50 nm×25 nm×25 nm, and (b) total energy against the calculation time for the three cases.

Figure 6. (a) Image of the final equilibrium states after MD running 50 ns for case 3 with the box size of 50 nm×50 nm×50 nm, analyzed by 3V method[32]: (b) surface of the particles at the probe radius, p=4 Å; (c) surface of the agglomerate at the probe

radius, p=4 nm; and (d) a schematic drawing of the space difference between the agglomerate volume (V_0, marked in blue) and the particle volume (V, marked in pink), which constitutes the primary pore space of the CLs.

Figure 7. The surface of (a) the Pt clusters, (b) the carbon slabs and (c) the Pt/C aggregate for the case 3 in the same equilibrium state after MD running for 50 ns. (d) a schematic diagram of the Pt and C interface, being applied to calculate the specific active area of the Pt clusters (A_s), when the total surface areas and the volumes are available, i.e., known A_1, V_1 from (a) and A_2, V_2 from (b), as well as A_{12}, V_{12} from (c).

Figure 8. Pair correlation functions (PCFs, or site-site radial distribution functions) between distinct components in CLs, representing the interactions for water (W-W), side chain of ionomer (S-S) and hydronium ions (Wh-Wh) in (a); and for other components with water in (b).

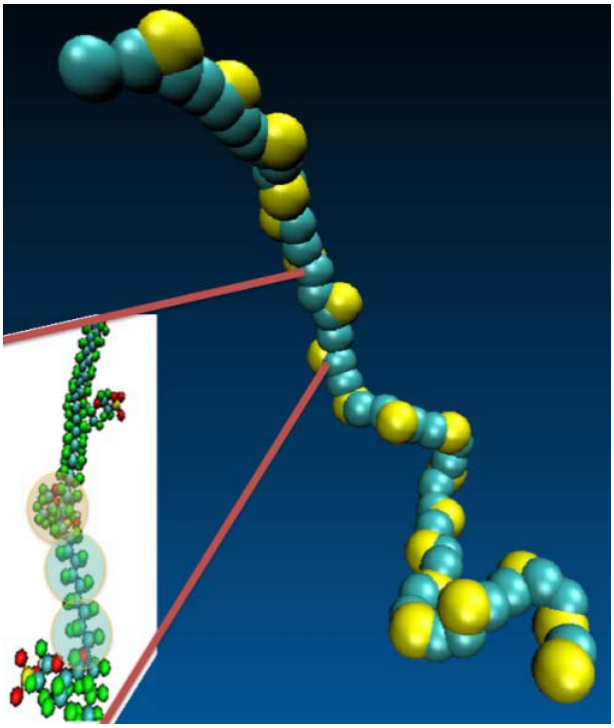

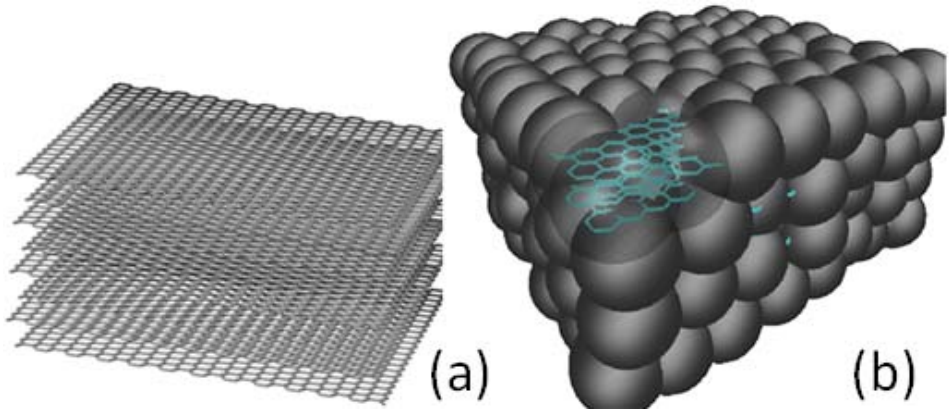
(a)
(b)

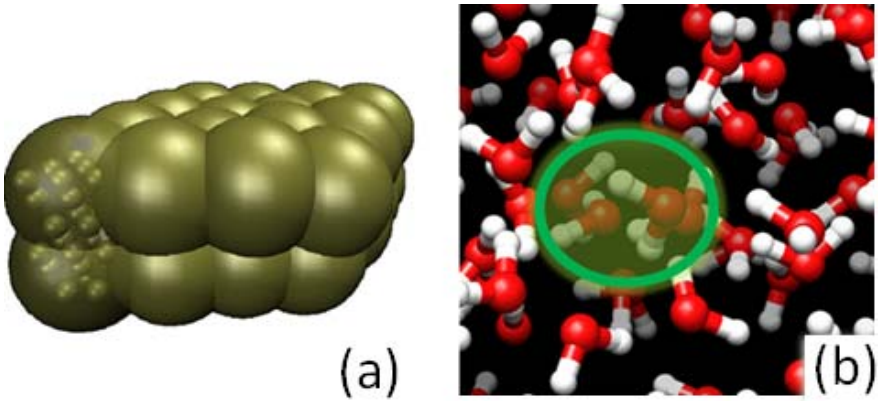
(a)
(b)

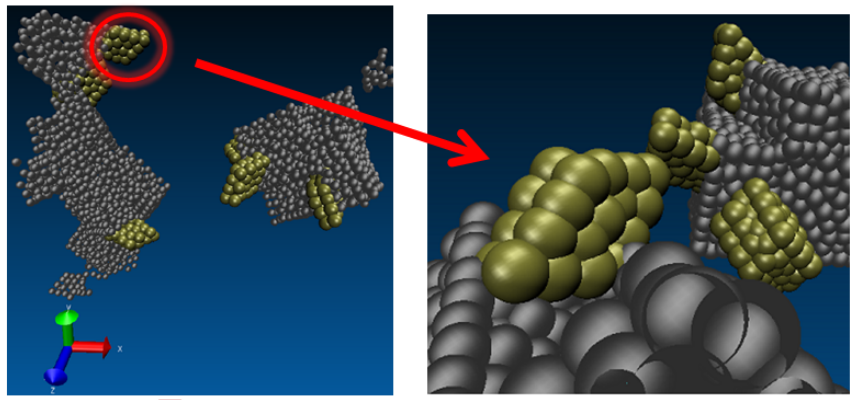

Step i: (a) (b)

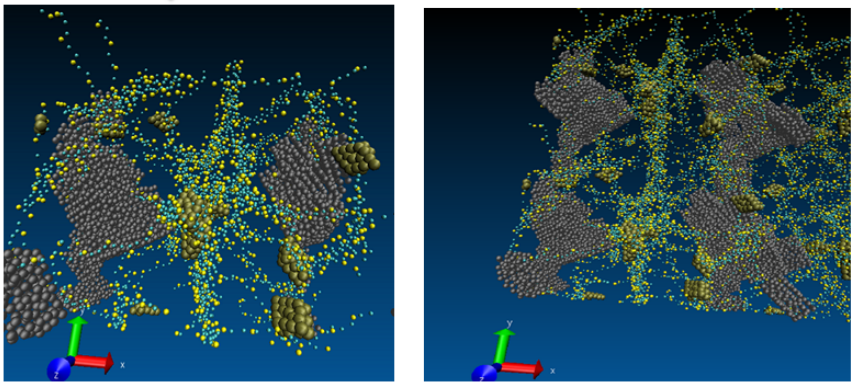

Step ii : (a) (b)

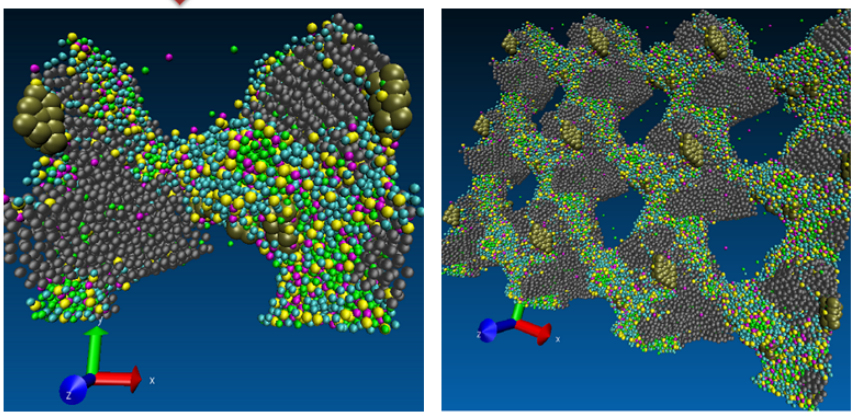

Step iii : (a) (b)

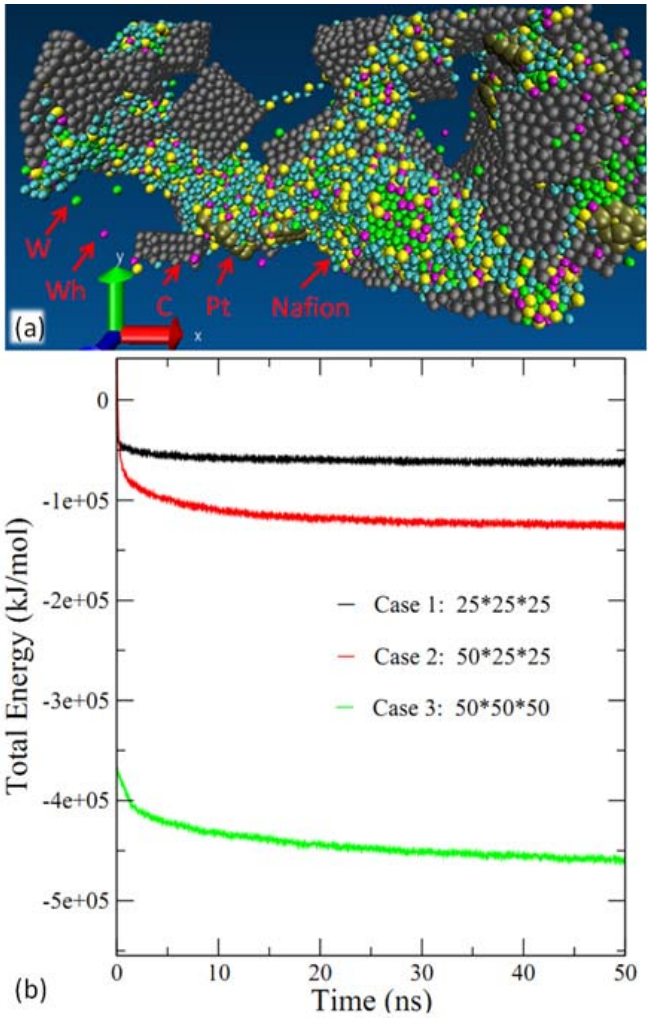
W
Wh
C
Pt
Nafion
(a)
y
x
0
-1e+05
-2e+05
-3e+05
-4e+05
-5e+05
Total Energy (kJ/mol)
Case 1: 25*25*25
Case 2: 50*25*25
Case 3: 50*50*50
0
10
20
30
40
50
Time (ns)
(b)

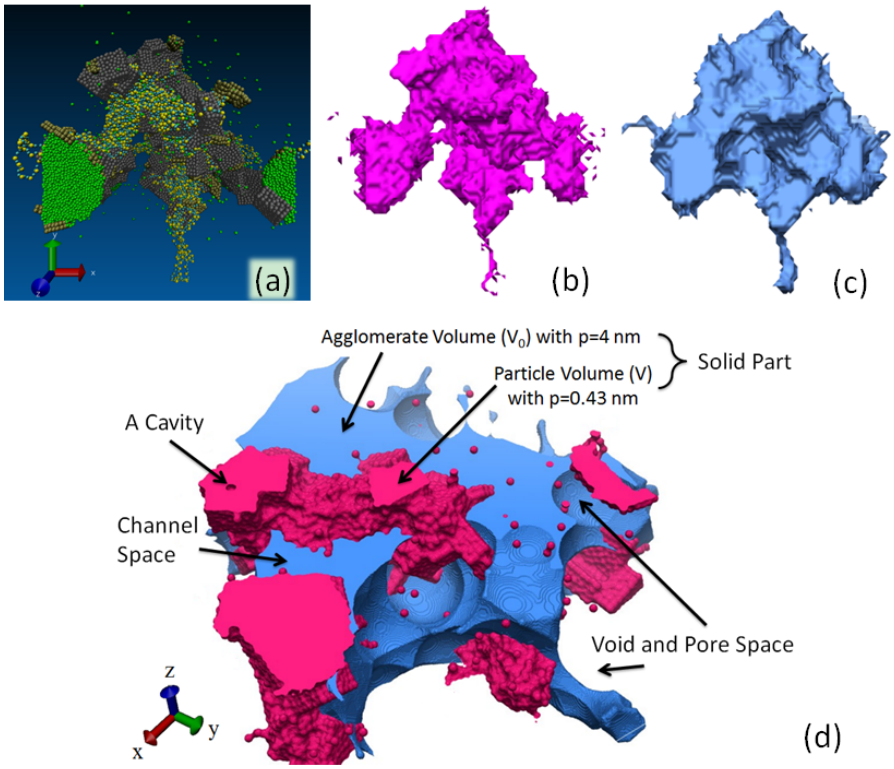
(a)
(b)
(c)
Agglomerate Volume (V_0) with p=4 nm
Particle Volume (V) with p=0.43 nm
Solid Part
A Cavity
Channel Space
Void and Pore Space
z
y
x
(d)

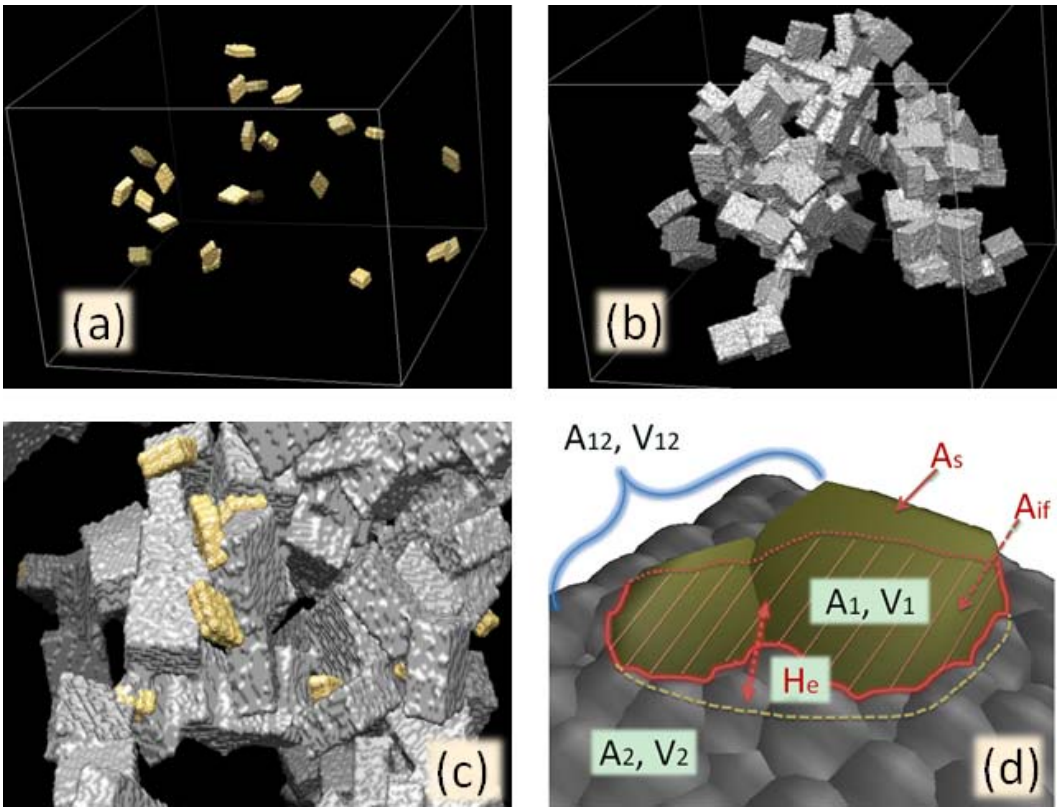
(a)
(b)
(c)
A12, V12
As
Aif
A1, V1
He
A2, V2
(d)

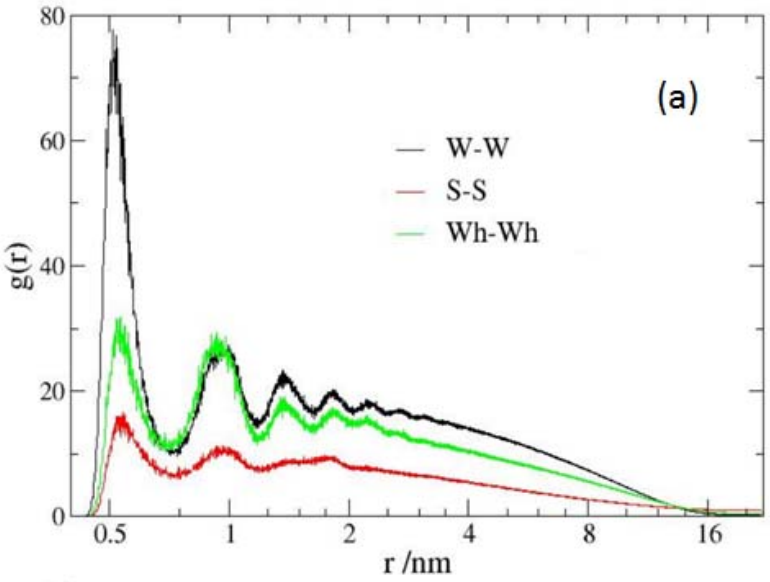
(a)
W-W
S-S
Wh-Wh
g(r)
r /nm
0
20
40
60
80
0.5
1
2
4
8
16

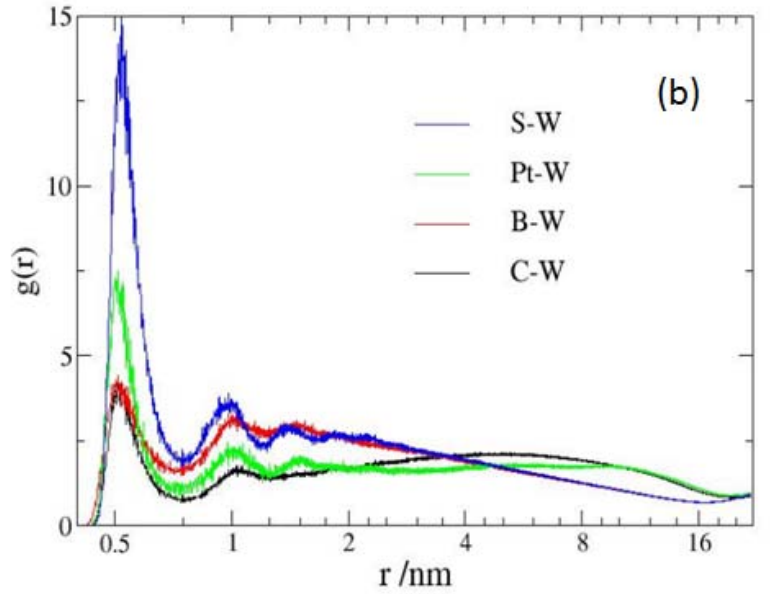
(b)
S-W
Pt-W
B-W
C-W
g(r)
r /nm
0
5
10
15
0.5
1
2
4
8
16